**Supporting Information**

# Back to the Future: Decomposability of a Biobased and Biodegradable Plastic in Field Soil Environments and Its Microbiome under Ambient and Future Climates

Witoon Purahong[1,*], Sara Fareed Mohamed Wahdan[1,2], Daniel Heinz[3], Katalee Jariyavidyanont[4], Chanita Sungkapreecha[4], Benjawan Tanunchai[1], Chakriya Sansupa[1], Dolaya Sadubsarn[1], Razan Alaneed[3], Anna Heintz-Buschart[1,5], Martin Schädler[5,6], Andreas Geissler[7], Joerg Kressler [3], François Buscot[1,5]

**Affiliations:**

[1]UFZ-Helmholtz Centre for Environmental Research, Department of Soil Ecology, Theodor-Lieser-Str. 4, D-06120 Halle (Saale), Germany; [2]Department of Botany, Faculty of Science, Suez Canal University, Ismailia, 41522, Egypt; [3]Department of Chemistry, Martin Luther University Halle-Wittenberg, D-06099 Halle (Saale), Germany; [4]Center of Engineering Sciences, Martin Luther University Halle-Wittenberg, Halle (Saale), Germany; [5]German Centre for Integrative Biodiversity Research (iDiv) Halle-Jena-Leipzig, Deutscher Platz 5e, D-04103 Leipzig, Germany; [6]UFZ-Helmholtz Centre for Environmental Research, Department of Community Ecology, Theodor-Lieser-Str. 4, D-06120 Halle (Saale), Germany. [7]Department of Macromolecular Chemistry and Paper Chemistry, Technical University of Darmstadt, Darmstadt D-64287, Germany.

**Number of pages**: 35

**Number of figures**: 15 (including 13 figures from Figure S1 – S13 and 2 figures presented in MATERIALS AND METHODS and Laboratory experiment)

**Number of tables**: 6 (including tables S1 – S3 presented in a separate excel file)

**Changes of biobased and biodegradable PBSA structure analysed with scanning electron microscope (SEM)**

In order to describe the chronology of polymer biodegradation, basically the three phases (colonization, enzymatic depolymerization and microbial utilization of the polymer carbon) can be differentiated [1]. Although these phases cannot be strictly separated in time with regard to the organisms identified and the structural changes in the PBSA material, decisive characteristics of these three stages can be determined for the sampling times of 30, 180 and 328 days. In the colonization phase, fungi initially appear as the dominant species. Relatively fast growing hyphae enable colonization of fresh substrates even over longer distances and do not necessarily depend on direct contact with the soil. The spread of bacteria, on the other hand, is usually dependent on passive transport through fluids (the existence of a water film) or on cell division. Hyphae that are spreading are able to adhere extremely tight to the substrate, so that they cannot be removed even by the described cleaning procedure. The spatial expansion of the hyphae as well as the potential for active mass transport enables the utilization of nutrient and moisture resources of a larger environment and makes the primary colonizer fungus more independent from local conditions.

The depolymerization symptoms, which can be observed after 180 days, occur, both on a large and localized scales (Supporting Information Fig. S2). While the extensive hydrolysis of the polymer surface begins in the amorphous polymer areas and, like an etching process, exposes areas of higher crystallinity, such a differentiation is not visible in the case of local corrosion. According to the electron microscope images, localized biocorrosion very often seems to originate in the immediate proximity of hyphae, which suggests the action of extracellular esterase (Fig. 1i, Supporting Information Fig. S3a and S3b). The spatially limited action of these enzymes leads to increased material removal and the formation of depressions. Since the

hydrolysis of each ester bond is accompanied by the release of a proton, a change in the pH value is to be expected especially in these depressions [2]. Developing local microclimates, both with regard to the pH value [2] and the moisture (Supporting Information Fig. S5) and oxygen supply [3], allow the settlement of more specialized microorganisms which further promotes the degradation. The heterogeneous distribution of the microorganisms on and in the polymer films causes an uneven material removal, which finally leads to perforation and fragmentation of the substrates.

As a smooth transition between the phases 2 and 3 mentioned above, microorganisms that are not involved in the depolymerization of the polymer, but that metabolize the increasingly released fragments (monomers and oligomers), are gradually settling on the substrate. The enlargement of the surface, which goes hand in hand with progressive biocorrosion, also offers these microorganisms increasing refuge. In the electron microscopic images of these samples, a large number of unicellular organisms can be observed, some of which are found in small groups or in large colonies on the substrate. Especially in this later phase of degradation (328 days), it is important to note the existence of distinct biofilms through which the organisms separate themselves from the environment (Supporting Information Fig. S3c and S3d). Interestingly, especially on these samples, traces of scavenging were found, which can most likely be attributed to the grazing of these biofilms by soil fauna not yet identified (Fig. 1j, Supporting Information Fig. S3e and S3f).

**Significant changes of weight and molar mass losses of biobased and biodegradable PBSA in natural field soil conditions analysed with gravimetric methods and gel permeation chromatography (GPC)**

Apart from microbial degradation, the abiotic environmental degradation (chemical mechanisms) may be also important to PBSA degradation [4]. The chemical degradation of

plastics in the environment requires water (hydrolysis) and oxygen (oxidation) and can be accelerated by microorganisms, heat, light or their combinations [4]. It would be valuable to know how much of the decomposition of the material that is caused by the microbial population, and how much is caused by physicochemical factors. We used the mass loss result at 328 days from a PBSA degradation experiment in extensively managed grassland plots to compare with the mass loss results in this study. The experiment in grassland and in conventional farming were located in the same experimental platform (GCEF) and have identical experimental design and setting (with ambient and future climate treatments). In the grassland plots, PBSA films were put on top of the grasses and thus had limited contact with the soil microbial community, such that the film was more influenced by physicochemical factors.

**Degradation of biobased and biodegradable PBSA as compared with plant litter materials**

The observed degradation of PBSA contrasts sharply with patterns in the decomposition of most leaf litter (exponential model with no or short lag phase) and is more similar to the observed pattern in low nitrogen (N) leaf litter and gymnosperm deadwood decomposition [5]. The longer lag phase of the PBSA degradation pattern as compared to leaf litter with sufficient amount of N can be explained by the different natures of the initial materials and the presence or absence of an established microbial community [5,6]. Leaf litter is made of readily available substrates such as sugars, starch and amino acids as well as larger complex substrates such as cellulose, hemi-cellulose and lignin [6]. Furthermore, it contains well established microbial communities (both bacteria and fungi) [7]. The leaf litter decomposition process by enzymatic activities of microbial endophytes and epiphytes as well as newly colonizing soil microbes starts already shortly after the leaves fall to the ground and causes rapid initial mass loss (short lag phase) [6–8]. Sufficient N content in leaf litter can reduce the lag phase, as fungi can use N as substrate for the production of a wide range of carbohydrate decomposing enzymes, including

endo-1,4-β-glucanase, endo-1,4-β-xylanase and β-1,4-glucosidase [9]. In contrast, at the onset of PBSA degradation, this substrate is characterized as a complex polymer with high carbon (C) content and without N and initial microbial community (Fig. 2) [10]. Microbes presumably need to establish N uptake from the soil or other sources [6]. Our results show that fungi maintained a certain biomass level across all sampling times from early to later degradation stages, while bacteria were almost absent at the early stage (30 days) of PBSA degradation (Fig. 2 c). Increases of bacterial abundance are only detected at the later stage of degradation. These results demonstrate that fungi may play an important role in triggering biodegradable plastic degradation, while bacteria play a role at later stages. No PCR products related to bacterial and fungal DNA could be detected in agarose gels in the initial PBSA samples, which demonstrates that the PBSA material used in this experiment was not previously colonized by microorganisms. This fact was also confirmed by real-time quantitative PCR (Fig. 2 c).

## MATERIALS AND METHODS

### Experimental setup and design

The study area is characterized by a subcontinental climate with average annual precipitations at 489 – 525 mm and mean temperature at 8.9 – 9.7 °C. The soil is classified as a Haplic Chernozem (highly fertile soil). The conventional farming plots are part of the GCEF, characterized by a typical regional crop rotation (including winter rape, winter wheat and winter barley) and application of mineral fertilizers and pesticides.

### Measurement of PBSA degradation

We determined both gravimetric weight and molar mass losses as proxies for the degradation rates of PBSA. The gravimetric weight loss alone is not evidence of polymer degradation as it can be caused by loss of additives and/or polymer fragments [11]. Degradation of a polymer has to occur through chain scission resulting in a decrease of its molar mass [11]. Gravimetric mass loss (Fig. 2) was determined on 12.5 $cm^2$ oven-dried PBSA samples (60 °C, 72 hr or until constant weight) using 5 digits balance (Mewes Wägetechnik, Haldensleben, Germany). The oven-dried PBSA samples from five replicates of ambient and future climates were cut into small pieces (<1 mm) and pooled to make a composite sample for each sampling time (0, 180 and 328 days). Five PBSA samples kept at room temperature with no soil contact for 328 days were oven-dried, cut, pooled and used as a negative control. Molar mass (Fig. 2) of each composite PBSA sample was determined using gel permeation chromatography (GPC) and presented as a number-average molecular weight ($M_n$ (g/mol)). The PBSA sample (3 – 5 mg) was dissolved in 1 – 1.5 mL N,N-dimethylformamide (DMF) solvent at 50 °C, then cooled down and filtered two times through a 0.2 µm polytetrafluoroethylene (PTFE) filter. From the sample, 20 µL was injected into the system at a flow rate of 1 mL/min. As solvent, DMF was

used with 10 mM lithium bromide (LiBr) at a temperature of 25 °C. For the analysis, the Viscotek instrument (GPC) was used in combination with a PSS PolarSil column (Polymer Standards Service, 300 Å, 5 µm, 8 x 300 mm) and the detection by the refractive index increment. Poly(methyl methacrylate) (PMMA) standards have been used as calibration standards. The measurements were conducted at room temperature. The polydispersity index (PDI) is calculated as the proportion between weight-average molecular weight ($M_w$ (g/mol)) and $M_n$ [12].

**PBSA microbiome**

The PBSA microbiome was characterized using rRNA operon amplicon sequencing by Illumina MiSeq. Sample processing for DNA extraction of PBSA buried in soil were modified from a protocol published elsewhere [13]. Briefly, we randomly cut 12.5 $cm^2$ PBSA samples and removed loosely adherent soil particles by vortexing in sterile phosphate-buffered saline (0.01M) for 5 min. PBSA samples were then submerged and shaken vigorously in 45 mL sterile Tween (0.1%) and this step was repeated 3 times. The samples were then washed 7 times using sterile water. Microbial biomass attached firmly with PBSA sample was then subjected to DNA extraction using DNeasy PowerSoil Kit (Qiagen, Hilden, Germany) with the aid of a Precellys 24 tissue homogenizer (Bertin Instruments, Montigny-le-Bretonneux, France). The presence and quantity of genomic DNA was checked using a NanoDrop ND-1000 spectrophotometer (Thermo Fisher Scientific, Dreieich, Germany) and the extracts were stored at -20 °C. Bacterial and fungal biomass (ng DNA/$cm^2$) was quantified using SYBR Green-based quantitative real-time polymerase chain reaction (qPCR) assays using the primer pairs (bacteria: Bac341f (5´-CCTACGGGNGGCWGCAG-3´) and Bac785r (5´-GACTACHVGGGTATCTAAKCC-3´) [14], annealing temperature: 53 °C; fungi: fITS7 (5′- GTGARTCATCGAATCTTTG-3′), and ITS4 primer (5′-TCCTCCGCTTATTGATATGC-3′) [15,16], annealing temperature: 54 °C. Tenfold

dilution standard series of genomic DNA of *Escherichia coli* K12 and soil fungus *Trichoderma guizhouense* were used to calibrate and calculate the bacterial and the fungal biomass (ng DNA/$cm^2$).

For bacterial and archaea amplicon library, the 16S rRNA gene V4 region was amplified using the universal bacteria/archaea primer pair 515F (5′ -GTGCCAGCMGCCGCGGTAA- 3′) and 806R (5′ -GGACTACHVGGGTWTCTAAT- 3′) [17] with Illumina adapter sequences. For the fungal amplicon libraries, the fungal internal transcribed spacer 2 (ITS2) gene was amplified using the fungal primer pair fITS7 (5′- GTGARTCATCGAATCTTTG-3′)[18] and ITS4 primer (5′-TCCTCCGCTTATTGATATGC-3′)[16] with Illumina adapter sequences. Amplifications were performed in 20 µL reactions with 5x HOT FIREPol Blend Master Mix (Solis BioDyne, Tartu, Estonia). Amplified products were visualized with gel electrophoresis and purified with an Agencourt AMPure XP kit (Beckman Coulter, Krefeld, Germany). Illumina Nextera XT Indices were added to both ends of the bacterial and fungal fragments. The products from 3 technical replicates were then pooled equimolar. Paired-end sequencing of 2 x 300 bp of this pool was performed using a MiSeq Reagent kit v3 on an Illumina MiSeq system (Illumina Inc., San Diego, CA, United States) at the Department of Soil Ecology, Helmholtz Centre for Environmental Research. The raw 16S and ITS rDNA sequences were deposited in the National Center for Biotechnology Information (NCBI) Sequence Read Archive (SRA) under study accession number PRJNA595487 (https://www.ncbi.nlm.nih.gov/bioproject/PRJNA595487).

The 16S and ITS rDNA raw sequence reads were first quality filtered for high quality reads from the paired-end sequences generated by the Illumina MiSeq sequencing platform using MOTHUR [19] and OBI Tools [20] software suits. Assembled reads fulfilling the following criteria were kept for further analyses: a minimum length of 200 nt (bacteria) or 120 nt (fungi); a minimum average quality of 25 Phred score for bacteria and fungi; containing homopolymers

with a maximum length of 20 nt; without ambiguous nucleotides. We detected chimeric sequences using the UCHIME algorithm [21] as implemented in MOTHUR and removed them from the datasets. The obtained reads were then clustered into operational taxonomic units (OTUs) using the CD-HIT-EST algorithm [22] at a threshold of 97% sequence similarity. The OTU representative sequences (defined as the most abundant sequence in each OTU) were taxonomically assigned against the reference sequences from the SILVA database v132 for prokaryote 16S [23] and from the UNITE database (version unite.v7) [24] for fungal ITS using the naive Bayesian classifier [25] as implemented in MOTHUR using the default parameters. Rare OTUs (singletons to tripletons), which potentially might represent artificial sequences were removed. The read counts were rarefied to the smallest read number per sample (31,141 and 26,056 reads for prokaryote (bacteria and archaea) and fungi, respectively). Microbial taxonomic and relative abundance information is provided in Supporting Information Table S1, S2 and S3. **Rarefaction curves of all the samples indicated sufficient sampling effort (Supporting Information Fig. S13), thus we used the observed richness as a measure of microbial diversity associated with PBSA degradation.** We checked the taxonomic annotation of top 20 highest relative abundant fungal OTUs used in this study by BLAST search against the current version of UNITE (version: 8.2; 2020-01-15) and UNITE species hypotheses [26] of each OTU is presented in Table S6. Ecological functions were determined for each OTU using FAPROTAX for bacteria and archaea [27], and FUNGuild [28] for fungi. Ecological functions of bacteria and archaea obtained by FAPROTAX were manually checked against other references for their present in soils.

*Rarefaction curves of prokaryotic (bacterial and archaeal) and fungal OTUs detected in this study.*

**Bacteria and archaea**

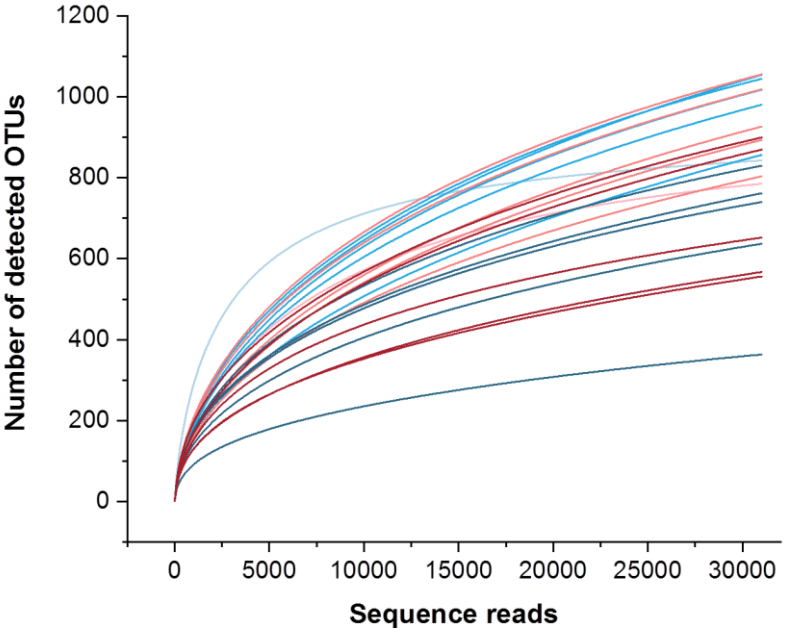


**Fungi**

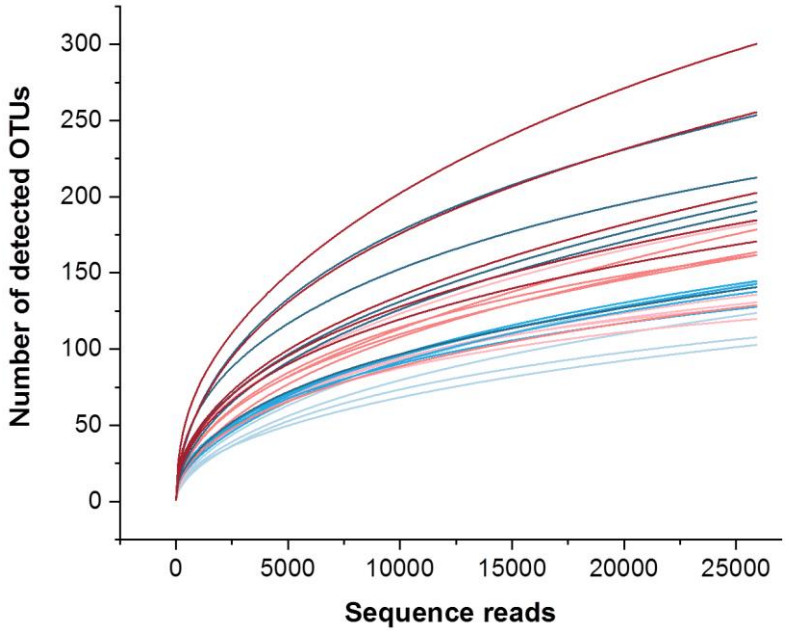

**Statistical analysis**

The effects of climate change treatments (ambient and future predicted climates) and sampling time (30, 180 and 328 days) on fungal and bacterial OTU richness and gravimetric mass remaining were analysed using two-way analysis of variance (ANOVA), incorporating the Jarque-Bera JB test for normality. The effects of climate change treatments and sampling time on bacterial and fungal community compositions were visualized using Non-metric multidimensional scaling (NMDS) based on the presence–absence data and Jaccard distance measure. Coloured ellipses in NMDS ordinations are 95% confidence intervals of species centroids for each treatment level. The effect of climate change treatments and sampling time on bacterial and fungal community compositions were determined using Permutational multivariate analysis of variance (PERMANOVA) based on the presence–absence data and Jaccard distance measure over 999 permutations. Since relative abundance data from metabarcoding may not be fully used quantitatively [29], we analysed the microbial community composition using both presence/absence and relative abundance data sets. The results from presence/absence data are presented in the main text and the corresponding results using relative abundance data (with the Bray–Curtis distance measure) are presented in Supporting Information Table S5. Differences between bacterial and fungal community compositions in soil and PBSA across different sampling times (0, 30, 180 and 328 days) were visualized and analysed using NMDS, PERMANOVA and Analysis of similarities (ANOSIM) based on the presence–absence data and Jaccard distance measure over 999 permutations. The effects of PBSA on soil water content and pH were analysed using paired *t*-test and *t*-test, incorporating the Jarque-Bera JB test for normality. Soil water content and pH data sets were checked for equality of variance using *F*-test. Interkingdom relationships at biomass and richness levels were tested using Pearson product-moment correlation coefficient whereas at the community

composition level the Mantel test was used. Correlations between the relative abundance of the most dominant known PBSA fungal degraders (*Cladosporium* OTU0002) as well as main PBSA coloniser (*Tetracladium* OTU0001) and relative abundance of symbiotic N fixing bacteria were tested using Spearman's rank correlation coefficient. All statistical analyses were performed using PAST version 2.17. NMDS visualization was performed using Vegan package of R version 3.2.2 [30].

## REFERENCES


(1) Sander, M. Biodegradation of Polymeric Mulch Films in Agricultural Soils: Concepts, Knowledge Gaps, and Future Research Directions. *Environ. Sci. Technol.* **2019**, *53* (5), 2304–2315. https://doi.org/10.1021/acs.est.8b05208.

(2) Gebauer, B.; Jendrossek, D. Assay of Poly(3-Hydroxybutyrate) Depolymerase Activity and Product Determination. *Appl. Environ. Microbiol.* **2006**, *72* (9), 6094–6100. https://doi.org/10.1128/AEM.01184-06.

(3) Ishigaki, T.; Sugano, W.; Nakanishi, A.; Tateda, M.; Ike, M.; Fujita, M. The Degradability of Biodegradable Plastics in Aerobic and Anaerobic Waste Landfill Model Reactors. *Chemosphere* **2004**, *54* (3), 225–233. https://doi.org/10.1016/S0045-6535(03)00750-1.

(4) Chamas, A.; Moon, H.; Zheng, J.; Qiu, Y.; Tabassum, T.; Jang, J. H.; Abu-Omar, M.; Scott, S. L.; Suh, S. Degradation Rates of Plastics in the Environment. *ACS Sustain. Chem. Eng.* **2020**, *8* (9), 3494–3511. https://doi.org/10.1021/acssuschemeng.9b06635.

(5) Cornwell, W. K.; Weedon, J. T. Decomposition Trajectories of Diverse Litter Types: A Model Selection Analysis. *Methods Ecol. Evol.* **2014**, *5* (2), 173–182. https://doi.org/10.1111/2041-210X.12138.

(6) Talbot, J. M.; Treseder, K. K. Interactions among Lignin, Cellulose, and Nitrogen Drive Litter Chemistry–Decay Relationships. *Ecology* **2012**, *93* (2), 345–354. https://doi.org/10.1890/11-0843.1.

(7) Purahong, W.; Wubet, T.; Lentendu, G.; Schloter, M.; Pecyna, M. J.; Kapturska, D.; Hofrichter, M.; Krüger, D.; Buscot, F. Life in Leaf Litter: Novel Insights into Community Dynamics of Bacteria and Fungi during Litter Decomposition. *Mol. Ecol.* **2016**, *25* (16), 4059–4074. https://doi.org/10.1111/mec.13739.

(8) Purahong, W.; Kapturska, D.; Pecyna, M. J.; Schulz, E.; Schloter, M.; Buscot, F.; Hofrichter, M.; Krüger, D. Influence of Different Forest System Management Practices on Leaf Litter Decomposition Rates, Nutrient Dynamics and the Activity of Ligninolytic Enzymes: A Case Study from Central European Forests. *PLoS ONE* **2014**, *9* (4), e93700. https://doi.org/10.1371/journal.pone.0093700.

(9) Lashermes, G.; Gainvors-Claisse, A.; Recous, S.; Bertrand, I. Enzymatic Strategies and Carbon Use Efficiency of a Litter-Decomposing Fungus Grown on Maize Leaves, Stems, and Roots. *Front. Microbiol.* **2016**, *7*. https://doi.org/10.3389/fmicb.2016.01315.

(10) Gigli, M.; Negroni, A.; Soccio, M.; Zanaroli, G.; Lotti, N.; Fava, F.; Munari, A. Influence of Chemical and Architectural Modifications on the Enzymatic Hydrolysis of Poly(Butylene Succinate). *Green Chem.* **2012**, *14* (10), 2885–2893. https://doi.org/10.1039/C2GC35876J.

(11) Albertsson, A.-C.; Hakkarainen, M. Designed to Degrade. *Science* **2017**, *358* (6365), 872–873. https://doi.org/10.1126/science.aap8115.

(12) Puchalski, M.; Szparaga, G.; Biela, T.; Gutowska, A.; Sztajnowski, S.; Krucińska, I. Molecular and Supramolecular Changes in Polybutylene Succinate (PBS) and Polybutylene Succinate Adipate (PBSA) Copolymer during Degradation in Various Environmental Conditions. *Polymers* **2018**, *10* (3), 251. https://doi.org/10.3390/polym10030251.

(13) Cosgrove, L.; McGeechan, P. L.; Robson, G. D.; Handley, P. S. Fungal Communities Associated with Degradation of Polyester Polyurethane in Soil. *Appl. Environ. Microbiol.* **2007**, *73* (18), 5817–5824. https://doi.org/10.1128/AEM.01083-07.

(14) Klindworth, A.; Pruesse, E.; Schweer, T.; Peplies, J.; Quast, C.; Horn, M.; Glöckner, F. O. Evaluation of General 16S Ribosomal RNA Gene PCR Primers for Classical and Next-Generation Sequencing-Based Diversity Studies. *Nucleic Acids Res.* **2013**, *41* (1), e1–e1. https://doi.org/10.1093/nar/gks808.

(15) Ihrmark, K.; Bödeker, I. T. M.; Cruz-Martinez, K.; Friberg, H.; Kubartova, A.; Schenck, J.; Strid, Y.; Stenlid, J.; Brandström-Durling, M.; Clemmensen, K. E.; Lindahl, B. D. New Primers to Amplify the Fungal ITS2 Region – Evaluation by 454-Sequencing of Artificial and Natural Communities. *FEMS Microbiol. Ecol.* **2012**, *82* (3), 666–677. https://doi.org/10.1111/j.1574-6941.2012.01437.x.

(16) White, T. J.; Bruns, T. D.; Lee, S.; Taylor, J. Amplification and Direct Sequencing of Fungal Ribosomal RNA Genes for Phylogenetics. In *Innis MA, Gelfand DH, Sninsky JJ,*

*White TJ (eds). PCR Protocols: A Guide to Methods and Applications.*; Academic Press: San Diego, 1990; Vol. 38, pp 315–322.

(17) Caporaso, J. G.; Lauber, C. L.; Walters, W. A.; Berg-Lyons, D.; Lozupone, C. A.; Turnbaugh, P. J.; Fierer, N.; Knight, R. Global Patterns of 16S RRNA Diversity at a Depth of Millions of Sequences per Sample. *Proc. Natl. Acad. Sci.* **2011**, *108* (Supplement 1), 4516–4522. https://doi.org/10.1073/pnas.1000080107.

(18) Ihrmark, K.; Bödeker, I. T. M.; Cruz-Martinez, K.; Friberg, H.; Kubartova, A.; Schenck, J.; Strid, Y.; Stenlid, J.; Brandström-Durling, M.; Clemmensen, K. E.; Lindahl, B. D. New Primers to Amplify the Fungal ITS2 Region – Evaluation by 454-Sequencing of Artificial and Natural Communities. *FEMS Microbiol. Ecol.* **2012**, *82* (3), 666–677. https://doi.org/10.1111/j.1574-6941.2012.01437.x.

(19) Schloss, P. D.; Westcott, S. L.; Ryabin, T.; Hall, J. R.; Hartmann, M.; Hollister, E. B.; Lesniewski, R. A.; Oakley, B. B.; Parks, D. H.; Robinson, C. J.; Sahl, J. W.; Stres, B.; Thallinger, G. G.; Van Horn, D. J.; Weber, C. F. Introducing Mothur: Open-Source, Platform-Independent, Community-Supported Software for Describing and Comparing Microbial Communities. *Appl. Environ. Microbiol.* **2009**, *75* (23), 7537–7541. https://doi.org/10.1128/AEM.01541-09.

(20) Boyer, F.; Mercier, C.; Bonin, A.; Le Bras, Y.; Taberlet, P.; Coissac, E. Obitools: A Unix-Inspired Software Package for DNA Metabarcoding. *Mol. Ecol. Resour.* **2016**, *16* (1), 176–182. https://doi.org/10.1111/1755-0998.12428.

(21) Edgar, R. C.; Haas, B. J.; Clemente, J. C.; Quince, C.; Knight, R. UCHIME Improves Sensitivity and Speed of Chimera Detection. *Bioinforma. Oxf. Engl.* **2011**, *27* (16), 2194–2200. https://doi.org/10.1093/bioinformatics/btr381.

(22) Fu, L.; Niu, B.; Zhu, Z.; Wu, S.; Li, W. CD-HIT: Accelerated for Clustering the next-Generation Sequencing Data. *Bioinforma. Oxf. Engl.* **2012**, *28* (23), 3150–3152. https://doi.org/10.1093/bioinformatics/bts565.

(23) Yilmaz, P.; Parfrey, L. W.; Yarza, P.; Gerken, J.; Pruesse, E.; Quast, C.; Schweer, T.; Peplies, J.; Ludwig, W.; Glöckner, F. O. The SILVA and "All-Species Living Tree Project (LTP)" Taxonomic Frameworks. *Nucleic Acids Res.* **2014**, *42* (D1), D643–D648. https://doi.org/10.1093/nar/gkt1209.

(24) Kõljalg, U.; Nilsson, R. H.; Abarenkov, K.; Tedersoo, L.; Taylor, A. F. S.; Bahram, M.; Bates, S. T.; Bruns, T. D.; Bengtsson-Palme, J.; Callaghan, T. M.; Douglas, B.; Drenkhan, T.; Eberhardt, U.; Dueñas, M.; Grebenc, T.; Griffith, G. W.; Hartmann, M.;

Kirk, P. M.; Kohout, P.; Larsson, E.; Lindahl, B. D.; Lücking, R.; Martín, M. P.; Matheny, P. B.; Nguyen, N. H.; Niskanen, T.; Oja, J.; Peay, K. G.; Peintner, U.; Peterson, M.; Põldmaa, K.; Saag, L.; Saar, I.; Schüßler, A.; Scott, J. A.; Senés, C.; Smith, M. E.; Suija, A.; Taylor, D. L.; Telleria, M. T.; Weiss, M.; Larsson, K.-H. Towards a Unified Paradigm for Sequence-Based Identification of Fungi. *Mol. Ecol.* **2013**, *22* (21), 5271–5277. https://doi.org/10.1111/mec.12481.

(25) Wang, Q.; Garrity, G. M.; Tiedje, J. M.; Cole, J. R. Naive Bayesian Classifier for Rapid Assignment of RRNA Sequences into the New Bacterial Taxonomy. *Appl. Environ. Microbiol.* **2007**, *73* (16), 5261–5267. https://doi.org/10.1128/AEM.00062-07.

(26) Nilsson, R. H.; Larsson, K.-H.; Taylor, A. F. S.; Bengtsson-Palme, J.; Jeppesen, T. S.; Schigel, D.; Kennedy, P.; Picard, K.; Glöckner, F. O.; Tedersoo, L.; Saar, I.; Kõljalg, U.; Abarenkov, K. The UNITE Database for Molecular Identification of Fungi: Handling Dark Taxa and Parallel Taxonomic Classifications. *Nucleic Acids Res.* **2019**, *47* (D1), D259–D264. https://doi.org/10.1093/nar/gky1022.

(27) Louca, S.; Parfrey, L. W.; Doebeli, M. Decoupling Function and Taxonomy in the Global Ocean Microbiome. *Science* **2016**, *353* (6305), 1272–1277. https://doi.org/10.1126/science.aaf4507.

(28) Nguyen, N. H.; Song, Z.; Bates, S. T.; Branco, S.; Tedersoo, L.; Menke, J.; Schilling, J. S.; Kennedy, P. G. FUNGuild: An Open Annotation Tool for Parsing Fungal Community Datasets by Ecological Guild. *Fungal Ecol.* **2016**, *20*, 241–248. https://doi.org/10.1016/j.funeco.2015.06.006.

(29) Amend, A. S.; Seifert, K. A.; Bruns, T. D. Quantifying Microbial Communities with 454 Pyrosequencing: Does Read Abundance Count? *Mol. Ecol.* **2010**, *19* (24), 5555–5565. https://doi.org/10.1111/j.1365-294X.2010.04898.x.

(30) Oksanen, J.; Blanche, F. G.; Friendly, M.; Kindt, R.; Legendre, P.; McGlinn, D.; Minchin, P. R.; O'Hara, R. B.; Simpson, G. L.; Solymos, P.; Stevens, M. H. H.; Szoecs, E.; Wagner, H. Vegan: Community Ecology Package. R-Package Version 2.4-0. 2016.

**How does the electron micrograph show that the film become non-crystalline?**

Like most polymers, the polyester PBSA is semicrystalline. This means that the material consists of both highly ordered (crystalline) and disordered (amorphous) domains. Although chemically identical, the arrangement of the polymer chains causes significant differences in material behaviour. The high degree of order of the polymer chains in the crystalline domains provides, among others, a higher density and a higher hardness. The resulting lower reactivity can be utilized to make the crystalline regions visible, e.g.: by means of etching processes. Biodegradation also proceeds (similar to chemical or physical etching) at different rates in amorphous and crystalline polymer regions. Under identical conditions, degradation processes preferentially take place in the amorphous regions. The polymer surface then appears increasingly rough to porous because the amorphous polymer areas are destroyed and dissolved out, while the crystalline areas, which are more difficult to degrade, accumulate. In the SEM images, for example in Figure S2, the resulting structures become visible. At least superficially, this degradation is accompanied by an increase in polymer crystallinity.

**Laboratory experiment demonstrates that *Tetracladium* spp. are important PBSA coloniser and potential decomposer.**

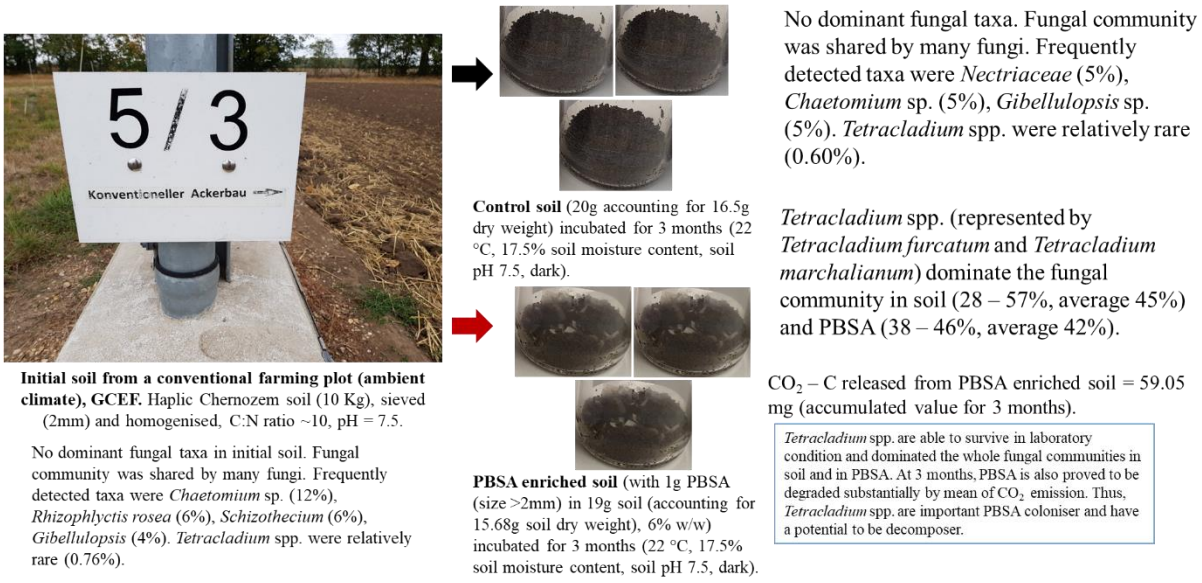


**Fungal communities in soils and PBSA samples** were characterized using Illumina sequencing as described in the Materials and methods section.

**Calculation of mineralized PBSA.**

Control and PBSA enriched soils were incubated in a Respicond V automatic respirometer (Nordgren Innovations AB, Sweden; Nordgren (1988) at a constant temperature of 22 °C, dark for 3 months.

The maximum fraction of PBSA - derived C in total $CO_2$ = Total $CO_2$ – $CO_2$ from control soil

**Reference:**

Nordgren A.Apparatus for the continuous, long-term monitoring of soil respiration ratein large numbers of samples. Soil Biol Biochem 1988; 20:955–7.

**Figure S1.** PBSA life cycle in soils.

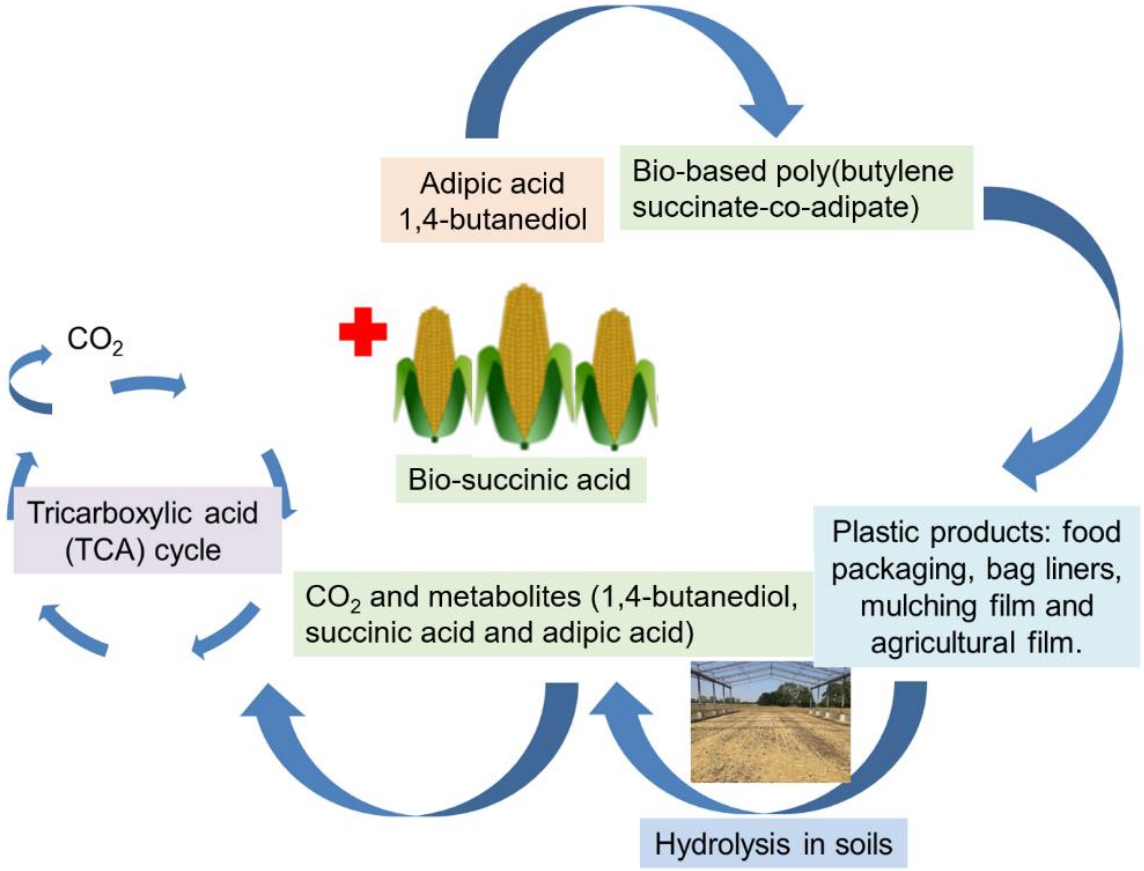

**Figure S2.** SEM images of virgin and corroded PBSA films. Fresh PBSA surface (a and b), extensive surface corrosion after 180 (c) and 328 (d) days of incubation, and localized corrosion patterns after 180 days (e and f).

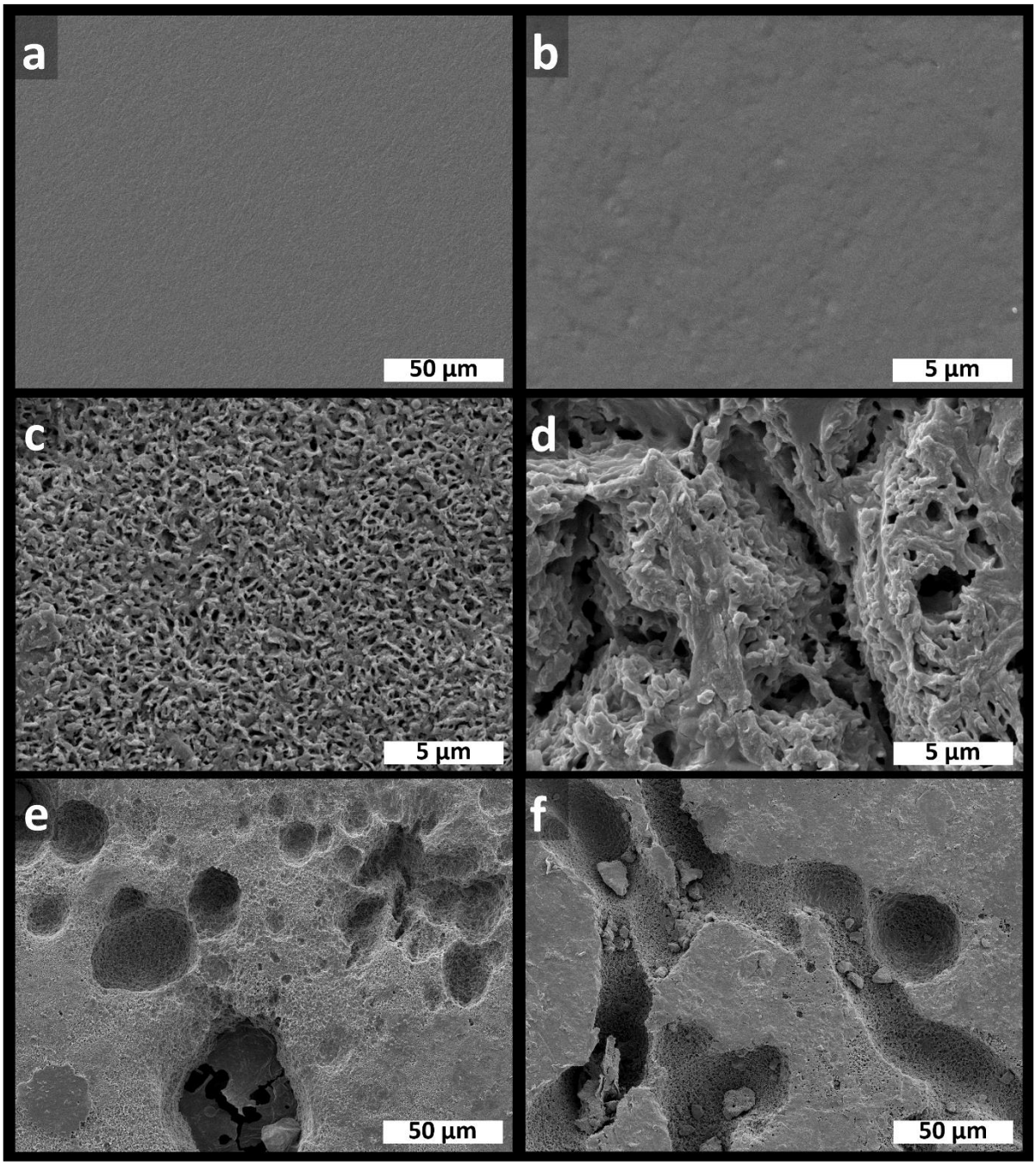

**Figure S3.** SEM images of PBSA surfaces. Shown in detail are hydrolytic polymer damage in the vicinity of fungal hyphae after 180 days (a, b) and large-area biofilms with a variety of bacteria (c, d) as well as traces of scavenging by unknown soil fauna after 328 days (e, f).

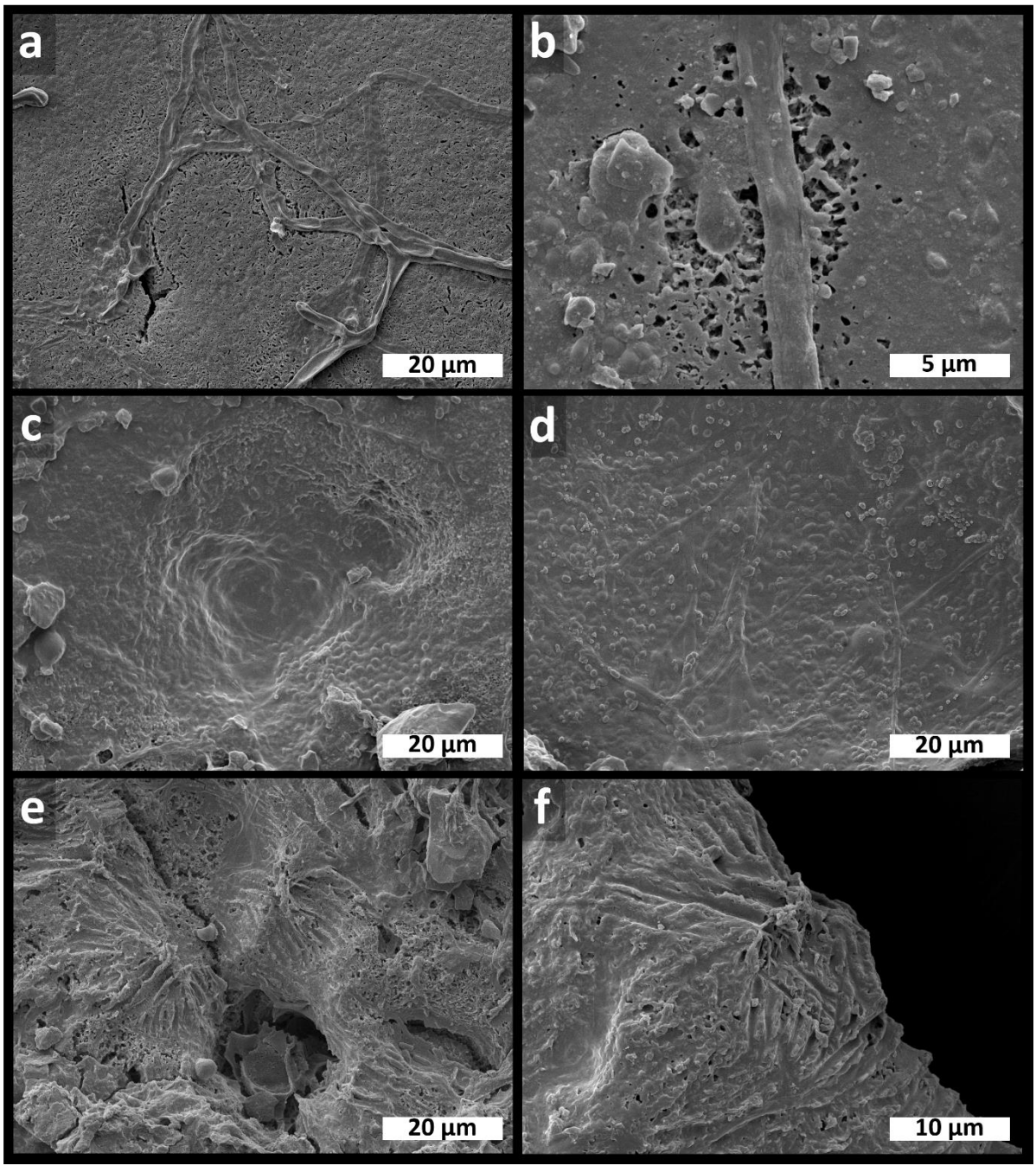

**Figure S4.** Changes of gravimetric and molar masses of 12.5 $cm^2$ poly(butylene succinate-co-adipate) (PBSA) film over 328 days in ambient (Amb) and future (Fut) climates. Gravimetric masses of PBSA at 0 day (initial stage) and 328 days at room temperature (without soil microbes) are also compared (bottom left panel).

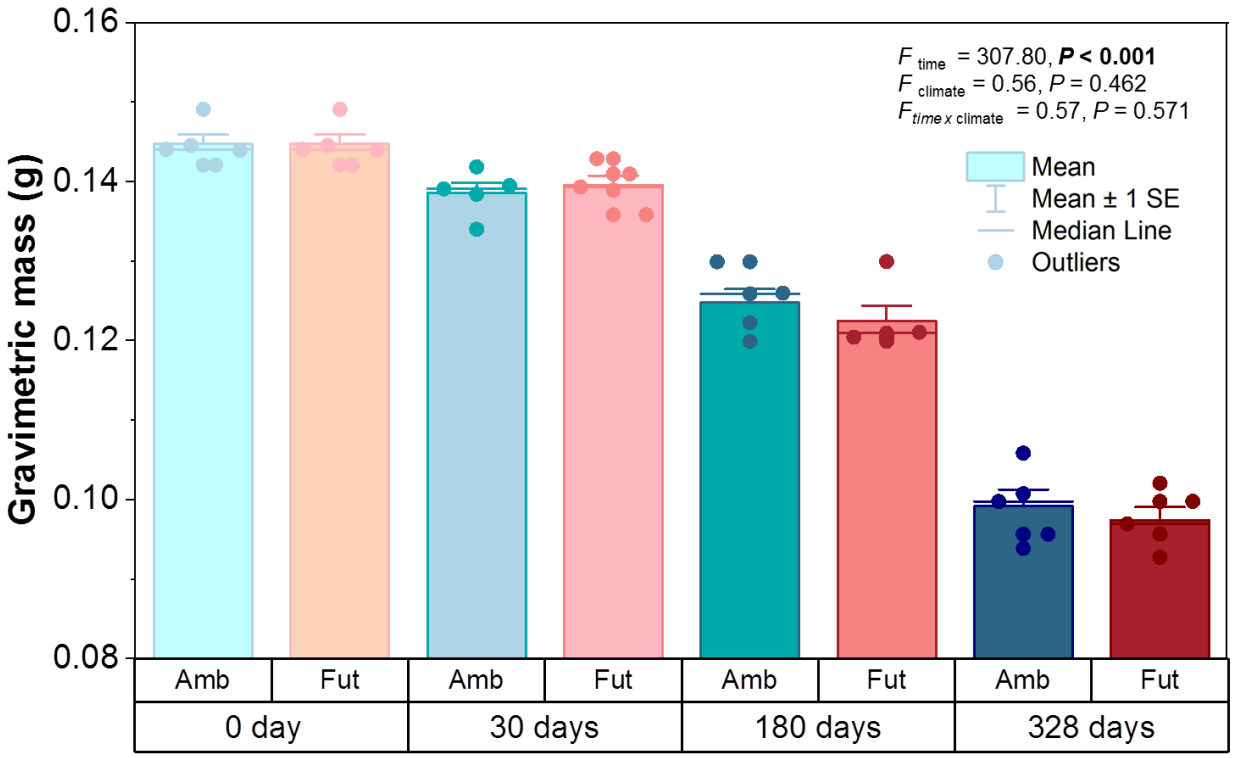


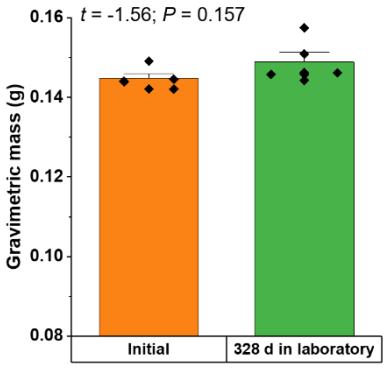


| Sample | Retention Volume (ml) | $M_n$ (g/mol) | PDI |
|---|---|---|---|
| Initial PBSA (0 day) | 7.733 | 92,400 | 2.90 |
| PBSA 328 days at room temperature (without soil microbes) | 7.917 | 88,100 | 3.16 |
| PBSA 180 days in ambient climate | 8.017 | 88,100 | 3.14 |
| PBSA 180 days in future climate | 7.917 | 89,700 | 3.03 |
| PBSA 328 days in ambient climate | 7.950 | 66,500 | 3.58 |
| PBSA 328 days in future climate | 7.883 | 64,000 | 3.73 |

**Figure S5.** Plot soil water content and soil water content under poly(butylene succinate-co-adipate) (PBSA) film after 328 days (mean ± SE). Different letters indicate significant different between means of the two treatments according to paired *t*-test ($t$ = 2.64, $P$ = 0.0270).

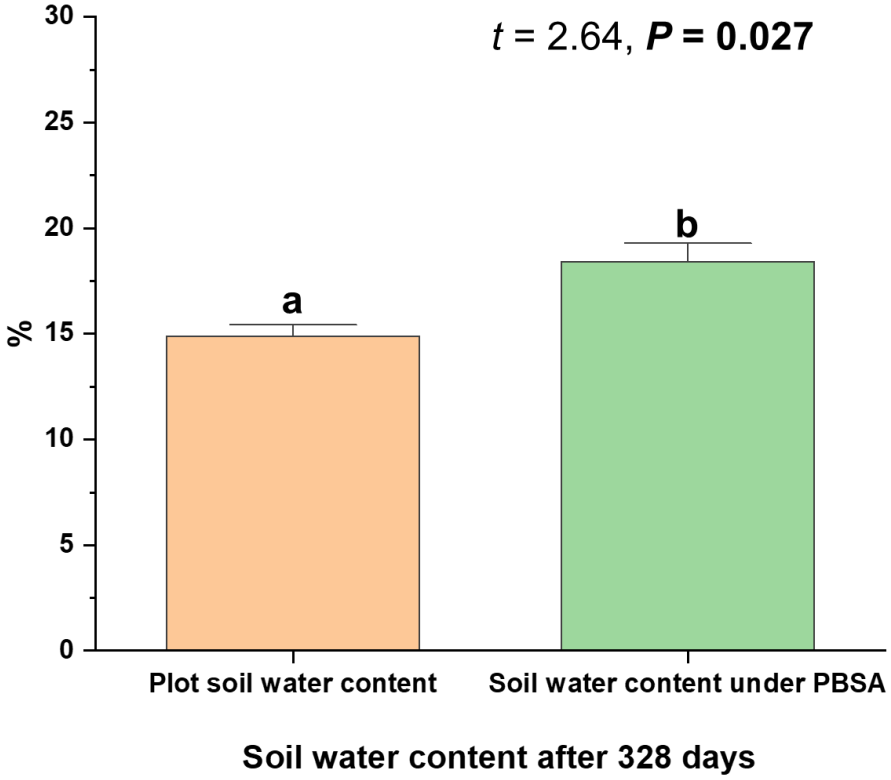

**Figure S6.** Red-Yellow-Green heat map with 50 percentile (yellow) represents average soil temperature (°C), average precipitation (mm/day) and average soil water content (%) of conventional farming plots under ambient and predicted future climate conditions during the experiment from August 2018 to August 2019.

| Incubation time | Time | Average soil temperature (°C) | | Average precipitation (mm/day) | | Average soil water content (%) | |
|---|---|---|---|---|---|---|---|
| | | Ambient | Future | Ambient | Future | Ambient | Future |
| 0 | 2018-08 | 23.0 | 23.8 | 0.252 | 0.307 | 4.0 | 3.0 |
| 30 | 2018-09 | 16.6 | 17.2 | 0.869 | 0.958 | 3.8 | 3.8 |
| 60 | 2018-10 | 10.9 | 11.8 | 0.277 | 0.222 | 9.5 | 11.8 |
| 90 | 2018-11 | 5.1 | 5.5 | 0.345 | 0.457 | - | - |
| 120 | 2018-12 | 3.8 | 3.9 | 1.097 | 1.042 | 15.9 | 16.2 |
| 150 | 2019-01 | 1.3 | 1.3 | 0.877 | 0.844 | - | - |
| 180 | 2019-02 | 3.1 | 3.0 | 0.104 | 0.089 | 19.9 | 19.7 |
| 210 | 2019-03 | 6.8 | 6.8 | 0.706 | 0.762 | - | - |
| 240 | 2019-04 | 9.9 | 10.0 | 0.493 | 0.562 | 15.0 | 15.3 |
| 270 | 2019-05 | 12.4 | 12.6 | 1.165 | 1.273 | - | - |
| 300 | 2019-06 | 21.3 | 21.8 | 0.673 | 0.603 | - | - |
| 328 | 2019-07 | 22.0 | 23.1 | 0.681 | 0.269 | 9.5 | 10.1 |
| 360 | 2019-08 | 21.3 | 22.2 | 0.567 | 0.695 | - | - |

**Figure S7.** Plot soil pH and soil pH (mean ± SE) under poly(butylene succinate-co-adipate) (PBSA) film after 328 days (a). Effect of PBSA addition (5% w/w) on soil pH after 90 days in laboratory condition (at 22 °C, soil water content 17.5%, dark) (b).

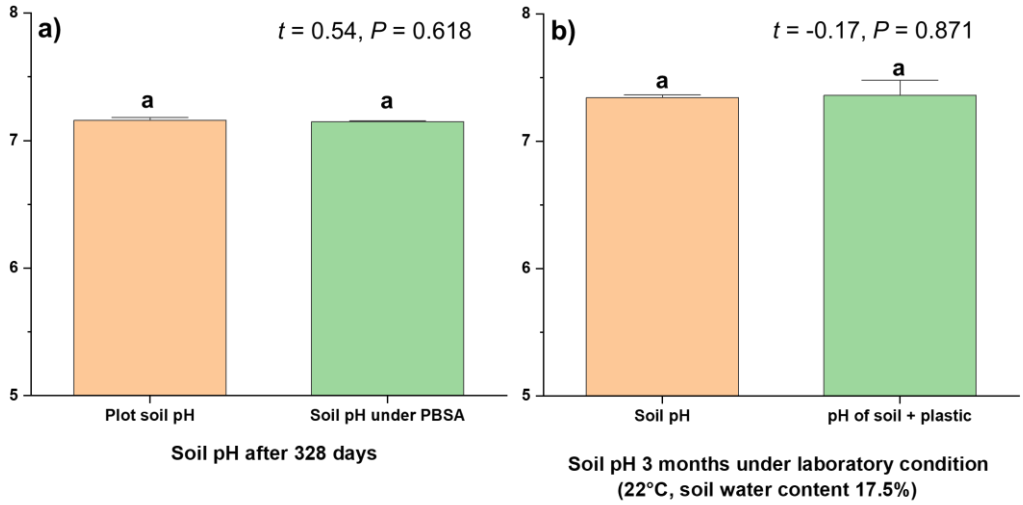

**Figure S8.** Detections of microbial communities in PBSA at 30 and 180 days.

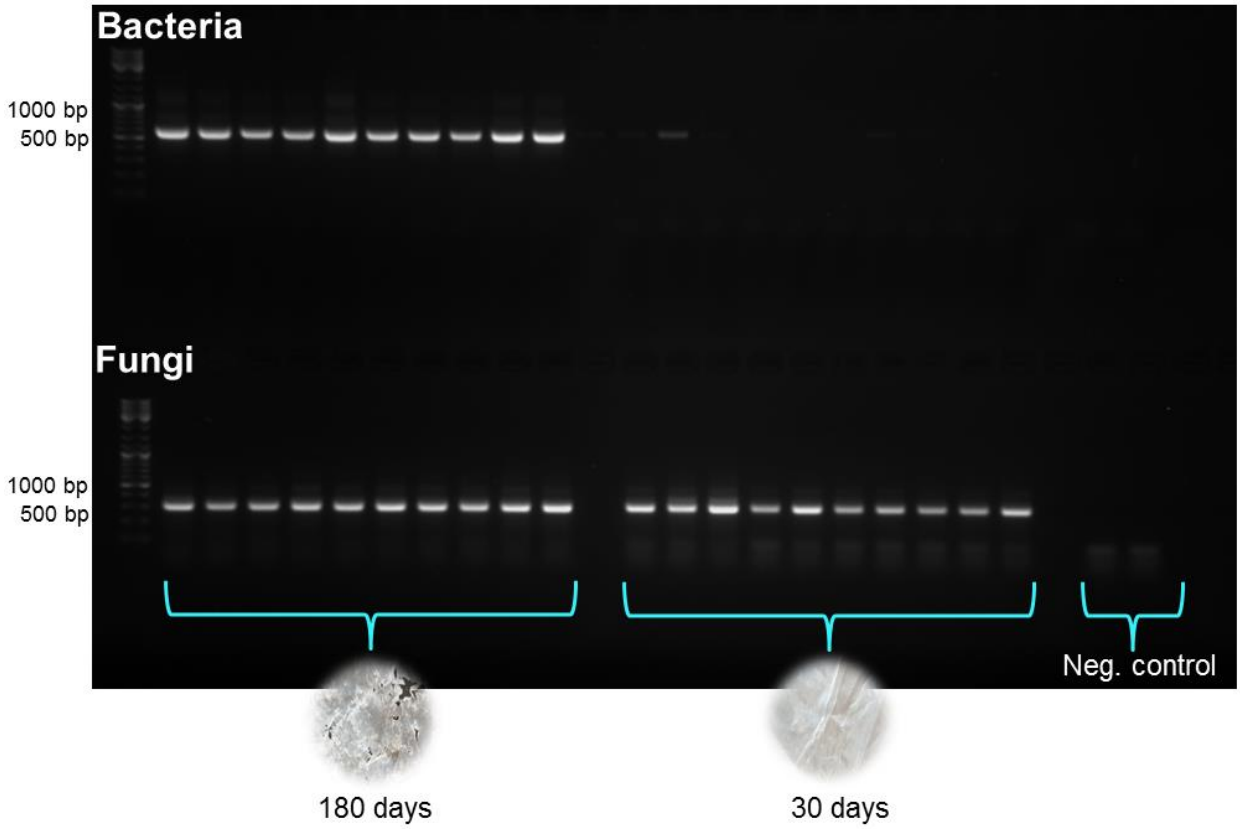

**Figure S9**. Composition of bacterial (a) and fungal (b) communities in PBSA and soil.

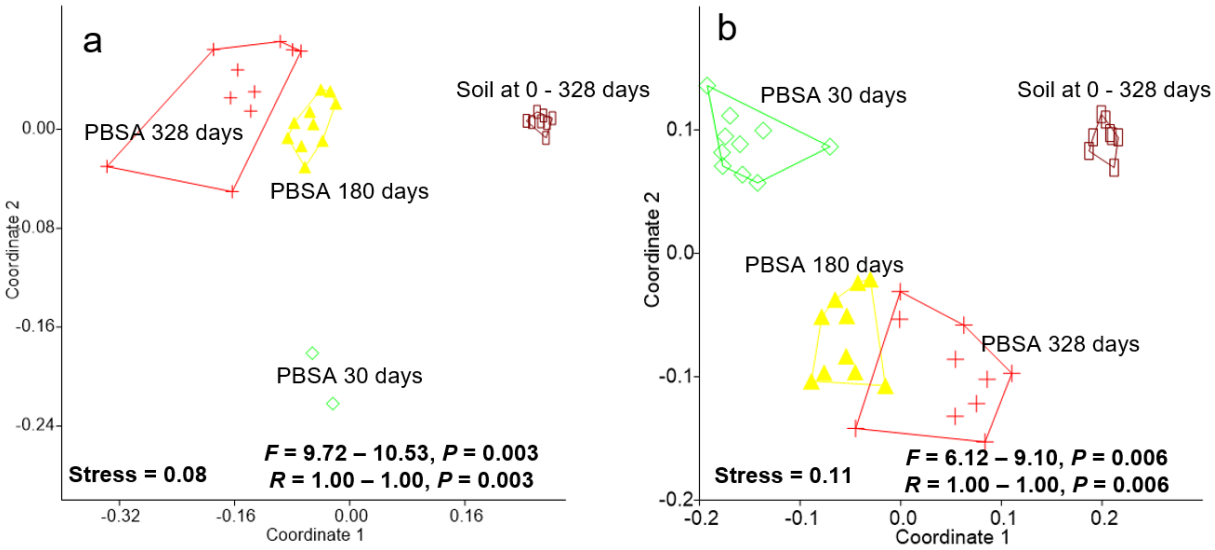


One-way nonparametric multivariate analysis of variance (NPMANOVA) and one-way analysis of similarities (ANOSIM) were used to test the differences in bacterial and fungal community composition between soil and PBSA samples using presence/absence data and Jaccard distances. Significance levels were based on 999 permutations. As more than two groups were compared, Bonferroni-corrected *P* values were applied. ANOSIM yields a sample statistic (*R*) indicating the degree of separation between test groups, with values ranging from −1 to 1 (*R* = 0–0.24, no separation to barely separated; *R* = 0.25–0.75, separation with different degrees of overlap; *R* > 0.75–1, well separated).

**Figure S10.** Microbes and their associated functions: heatmap (relative abundance of the successfully functional assignment OTUs based on FAPROTAX, FUNGuild and a database for bioplastics-degrading microorganisms) of potential functions of prokaryotes (archaea and bacteria (a) and fungi (e); cluster analysis based on relative abundance of the successfully functional assignment OTUs displays the functional succession throughout the two climate treatments (blue: ambient (A) and rose-red: future (F)) and three sampling times (30, 180 and 328 days) of prokaryotes (b) and fungi (f); heatmap of microbial taxa (prokaryotes (c) and fungi (g)) associated functions (number of sequence reads detected from the successfully functional assignment microbial genera or families, minimum sequence reads from normalized data sets are 200 for prokaryotes and 100 for fungi; Potential symbiotic and non-symbiotic nitrogen-fixing bacteria in PBSA samples and their associated sequence reads from normalized data sets (d); UNITE species hypotheses (Nilsson et. al., 2019) and current names of the two most detected fungal OTUs (h). *Cladosporium* spp. and *Fusarium solani* were identified using additional references as PBS based plastics degraders (Emadian et. al., 2017). Apart from figure S10d, other potential nitrogen-fixing bacterial genera detected in PBSA samples were *Bosea*, *Allorhizobium*, *Neorhizobium*, *Pararhizobium*, *Aminobacter*, *Mesorhizobium*, *Phyllobacterium*, *Shinella* (Sansupa et. al., 2021; Velázquez et. al., 2017). List of all archaea, bacteria and fungi (with their potential functions assigned by FAPROTAX or FUNGuild) are presented in Tables S1–S3. PBS based plastics degraders and N fixation were added to the functions assigned by FAPROTAX and FUNGuild as stated in "Material and Methods".

**Figure S10.** Continued.

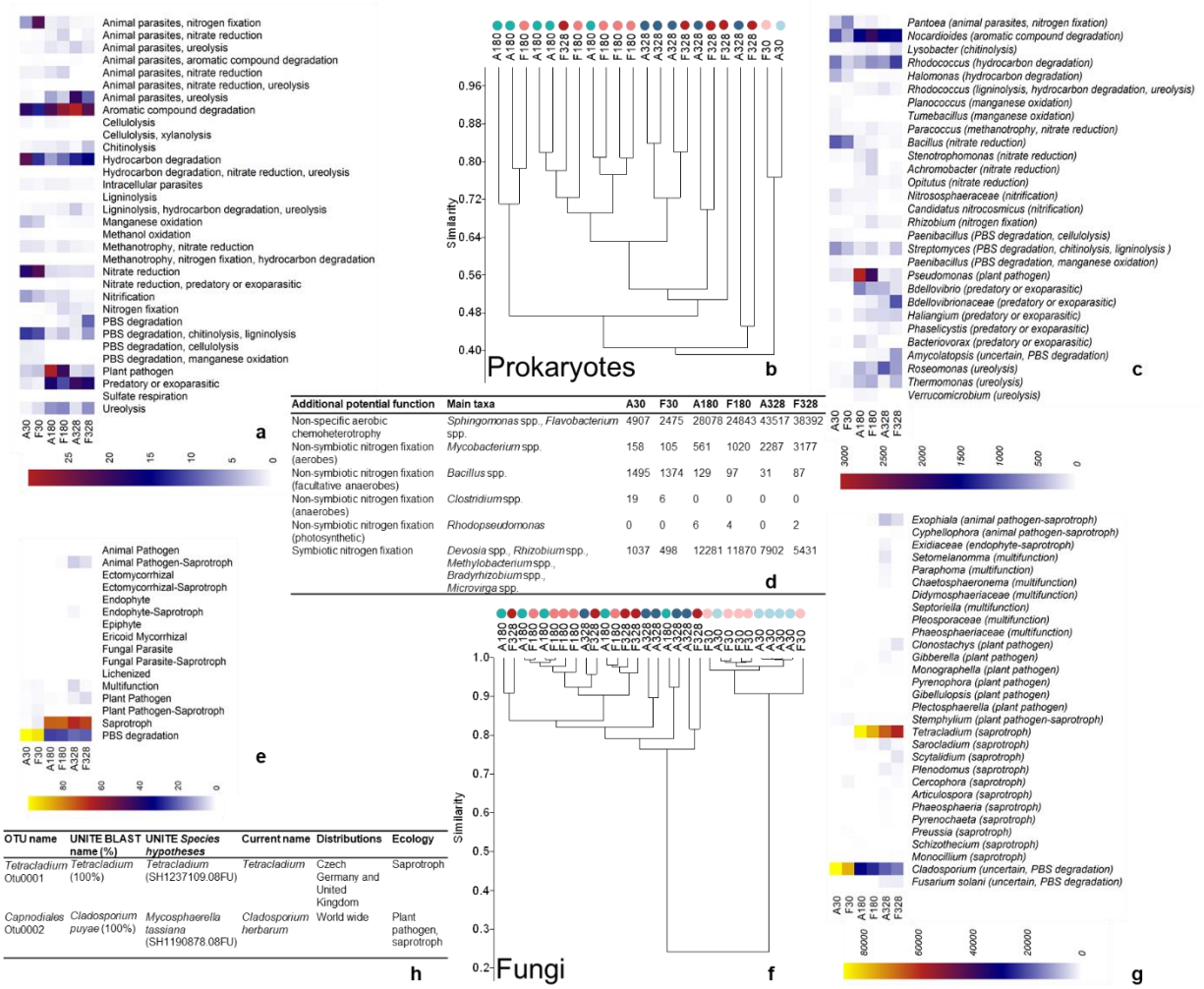


## References


Emadian, S. M.; Onay, T. T.; Demirel, B. Biodegradation of Bioplastics in Natural Environments. Waste Manage. 2017, 59, 526−536.

Nilsson, R. H.; Larsson, K.-H.; Taylor, A. F. S.; Bengtsson-Palme, J.; Jeppesen, T. S.; Schigel, D.; Kennedy, P.; Picard, K.; Glöckner, F. O.; Tedersoo, L.; Saar, I.; Kõljalg, U.; Abarenkov, K. The UNITE Database for Molecular Identification of Fungi: Handling Dark Taxa and Parallel Taxonomic Classifications. *Nucleic Acids Res.* **2019**, *47* (D1), D259–D264. https://doi.org/10.1093/nar/gky1022.

Sansupa, C.; Wahdan, S.F.M.; Hossen, S.; Disayathanoowat, T.; Wubet, T.; Purahong, W. Can we use functional annotation of prokaryotic taxa (FAPROTAX) to assign the ecological functions of soil bacteria? Appl. Sci. 2021, 11, 688.

Velázquez, E.; García-Fraile, P.; Ramírez-Bahena, M.H.; Rivas, R.; Martínez-Molina, E. Current Status of the Taxonomy of Bacteria Able to Establish Nitrogen-Fixing Legume Symbiosis. In Microbes for Legume Improvement; Springer Science and Business Media LLC: Cham, Switzerland, 2017; pp. 1–43.

**Figure S11:** Simplified microbial taxonomic and functional community dynamics in poly(butylene succinate-co-adipate) (PBSA) microbiome system. **Archaea**: can, *Candidatus nitrocosmicus*; ni, Nitrososphaeraceae, **bacteria**: ac, *Achromobacter*; am, *Amycolatopsis*; ba, *Bacillus*; bac, *Bacteriovorax*; bd, *Bdellovibrio* or Bdellovibrionaceae; br, *Bradyrhizobium*; de, *Devosia*; fl, *Flavobacterium*; ha, *Halomonas*; hal, *Haliangium*; ly, *Lysobacter*; me, *Methylobacterium*; my, *Mycobacterium*; no, *Nocardioides*; op, *Opitutus*; pae, *Paenibacillus*; pan, *Pantoea*; ps, *Pseudomonas*; rh, *Rhodococcus*; rhi, *Rhizobium*; ro, *Roseomonas*; sp, *Sphingomonas*; ste, *Stenotrophomonas*; str, *Streptomyces*; th, *Thermomonas*, **fungi**: ce, *Cercophora*; cl, *Cladosporium*; ex, *Exophiala*; fu, *Fusarium solani*; pu, *Purpureocillium*; st, *Stemphylium*; te, *Tetracladium*.

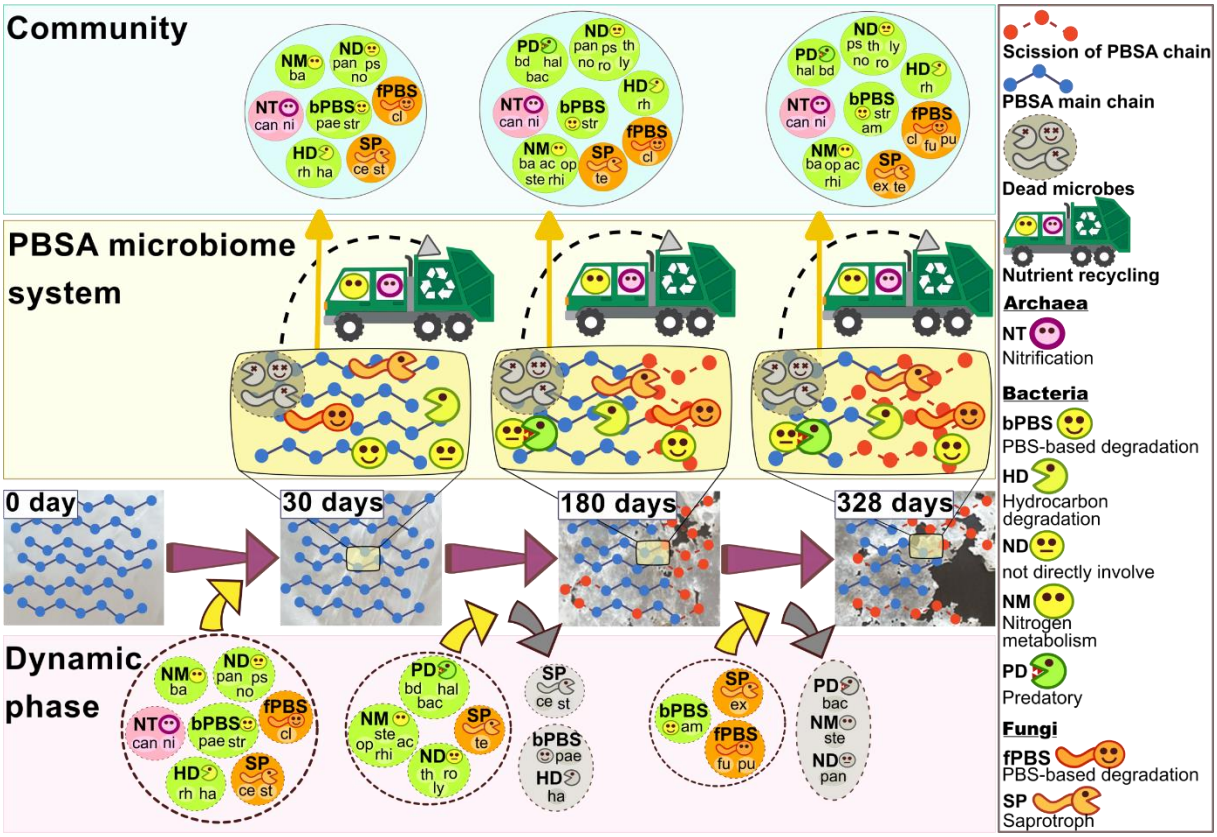

**Figure S12.** Detections of *nifH* gene in poly(butylene succinate-co-adipate) (PBSA) at 180 and 328 days.

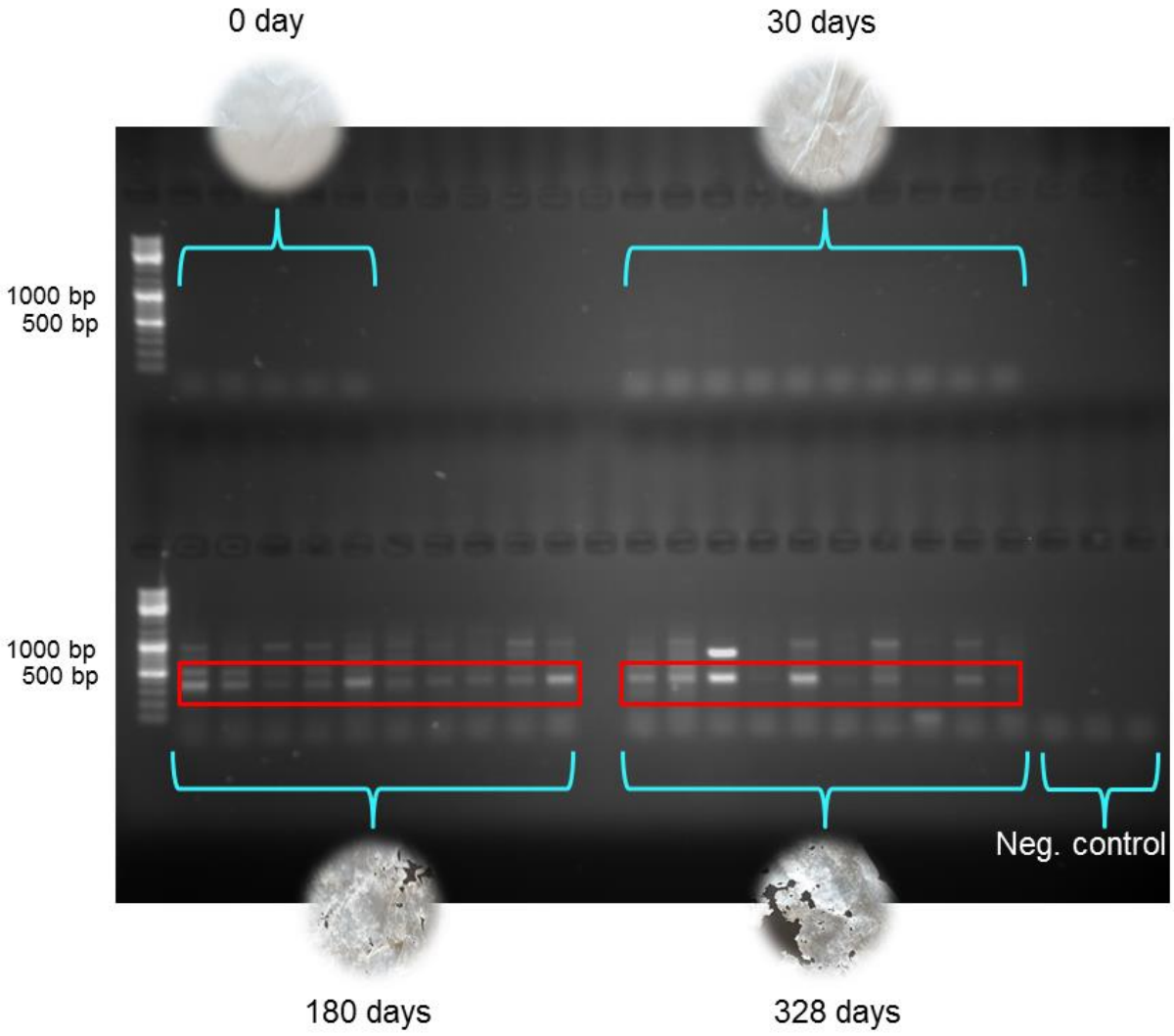

**Figure S13.** Correlations between the relative abundance of the most dominant known PBSA fungal degraders (*Cladosporium* OTU0002) as well as main PBSA coloniser (*Tetracladium* OTU0001) and relative abundance of symbiotic N fixing bacteria.

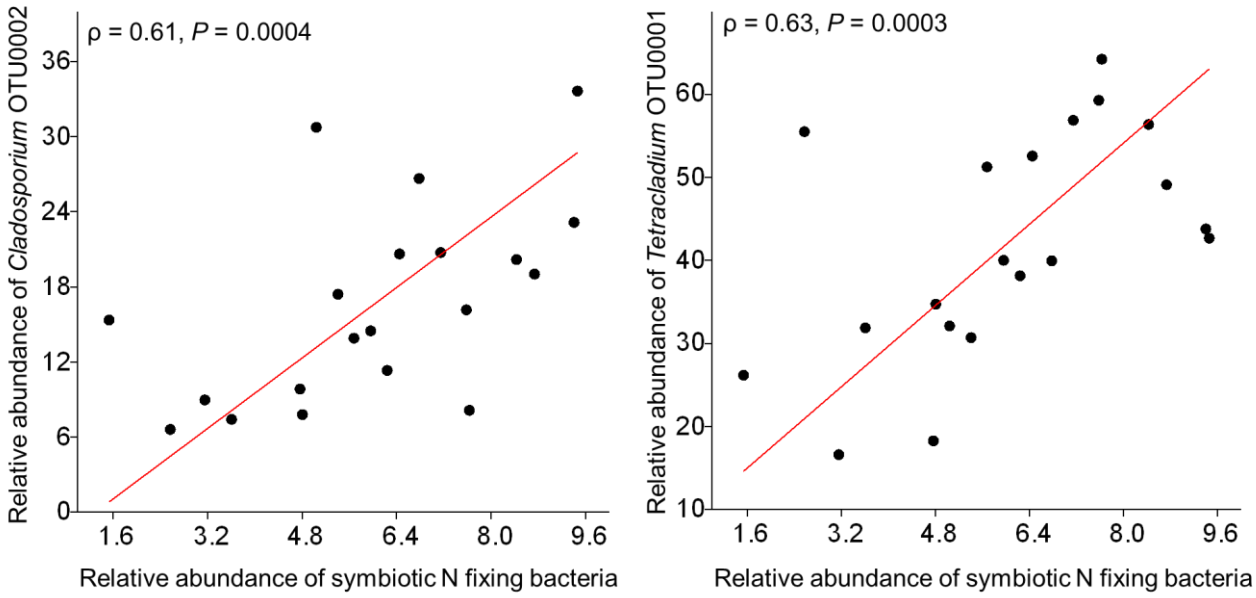

**Table S1.** Information on archaeal OTUs detected in poly(butylene succinate-co-adipate) (PBSA).

**Table S2.** Information on bacterial OTUs detected in poly(butylene succinate-co-adipate) (PBSA).

**Table S3.** Information on fungal OTUs detected in poly(butylene succinate-co-adipate) (PBSA).

**(Tables S1 – S3 are presented in a separate excel file).**

**Table S4.** Top 20 highest relative abundant fungal OTUs by BLAST search against the current version of UNITE (version 2.8, 2020-01-15) and UNITE species hypotheses (SH, at 3% threshold). Percent similarity ranges from 98 – 100%.

| OTU | Average relative abundance | UNITE species hypotheses | %similarity | SH |
|---|---|---|---|---|
| Otu0002 | 32.10 | *Cladosporium (Mycosphaerella tassiana)* | 100 | SH1190878.08FU |
| Otu0001 | 28.02 | *Tetracladium* | 100 | SH1237109.08FU |
| Otu0003 | 7.51 | *Alternaria alternata (Alternaria planifunda)* | 100 | SH1157990.08FU |
| Otu0005 | 6.42 | *Alternaria infectoria (Alternaria metachromatica)* | 100 | SH1142798.08FU |
| Otu0004 | 4.90 | *Tetracladium* | 100 | SH1237102.08FU |
| Otu0006 | 3.52 | *Tetracladium maxilliforme* | 100 | SH1237102.08FU |
| Otu0008 | 2.33 | *Epicoccum nigrum (Didymella exigua)* | 100 | SH1174007.08FU |
| Otu0009 | 1.64 | *Pseudogymnoascus pannorum (Pseudogymnoascus roseus)* | 100 | SH1180708.08FU |
| Otu0007 | 1.36 | *Exophiala equina* | 100 | SH1185366.08FU |
| Otu0010 | 0.99 | *Coniothyrium cereale (Neosetophoma rosigena)* | 100 | SH1157057.08FU |
| Otu0011 | 0.63 | *Sarocladium strictum* | 100 | SH1170554.08FU |
| Otu0014 | 0.53 | *Fusarium merismoides (Fusicolla aquaeductuum)* | 100 | SH1173595.08FU |
| Otu0021 | 0.47 | *Aureobasidium pullulans* | 100 | SH1149661.08FU |
| Otu0019 | 0.46 | *Chaetomium globosum (Chaetomium grande)* | 100 | SH1215738.08FU |
| Otu0012 | 0.43 | *Fusarium solani (Fusarium pseudensiforme)* | 100 | SH1173587.08FU |
| Otu0013 | 0.43 | *Clonostachys rosea* | 100 | SH1155535.08FU |
| Otu0017 | 0.41 | *Fusarium (Fusarium proliferatum)* | 100 | SH1212031.08FU |
| Otu0015 | 0.38 | *Scytalidium (Pezizomycotina)* | 100 | SH1185583.08FU |
| Otu0016 | 0.37 | *Acremonium sclerotigenum ( Pezizomycotina)* | 100 | SH1182823.08FU |
| Otu0018 | 0.34 | *Setomelanomma ( Setomelanomma holmii)* | 100 | SH1216099.08FU |
| Otu0020 | 0.29 | *Leptosphaeria biglobosa (Plenodomus biglobosus)* | 98 | SH1158458.08FU |
| Otu0025 | 0.28 | *Fusarium* | 100 | SH1173621.08FU |
| Otu0029 | 0.22 | *Stemphylium vesicarium* | 100 | SH1157993.08FU |
| Otu0027 | 0.22 | *Cladorrhinum samala* | 100 | SH1142221.08FU |
| Otu0022 | 0.20 | *Pyrenochaetopsis decipiens ( Pyrenochaetopsis leptospora)* | 100 | SH1157053.08FU |
| Otu0024 | 0.20 | *Fusarium avenaceum (Gibberella tricincta)* | 100 | SH1173588.08FU |
| Otu0023 | 0.19 | Exidiaceae | 98 | SH1212226.08FU |
| Otu0026 | 0.16 | *Cylindrocarpon* | 100 | SH1184595.08FU |
| Otu0030 | 0.14 | *Alternaria (Alternaria metachromatica)* | 100 | SH1142798.08FU |
| Otu0028 | 0.13 | *Monographella nivalis* | 100 | SH1179475.08FU |
| Otu0035 | 0.13 | *Alternaria (Alternaria planifunda)* | 99 | SH1157990.08FU |

**Table S5.** Statistical support for microbial richness and community composition in poly(butylene succinate-co-adipate) (PBSA).

| **Microbial Kingdom** | **Factor** | **Richness analysis (2-way ANOVA)** | | **Community analysis (2-way PERMANOVA), presence/absence** | | **Community analysis (2-way PERMANOVA), relative abundance** | |
|---|---|---|---|---|---|---|---|
| | | *F* | *P* | Pseudo*F* | *P* | Pseudo*F* | *P* |
| Archaea | Sampling time | 39.00 | **<0.001** | 5.56 | **0.001** | 3.66 | **0.004** |
| | Climate | 1.30 | 0.279 | 1.79 | *0.090* | 2.20 | *0.058* |
| | Sampling time x Climate | 0.03 | 0.875 | 1.83 | 0.103 | 2.97 | **0.012** |
| Bacteria | Sampling time | 19.95 | **<0.001** | 3.23 | **0.001** | 6.61 | **0.001** |
| | Climate | 0.01 | 0.946 | 0.99 | 0.432 | 1.27 | 0.267 |
| | Sampling time x Climate | 0.57 | 0.462 | 0.83 | 0.842 | 0.32 | 0.984 |
| Fungi | Sampling time | 50.48 | **<0.001** | 3.88 | **0.001** | 33.80 | **0.001** |
| | Climate | 3.33 | *0.081* | 1.23 | 0.107 | 1.47 | 0.235 |
| | Sampling time x Climate | 0.09 | 0.912 | 1.00 | 0.363 | 0.81 | 0.491 |

**Table S6.** Carbon (C), nitrogen (N) and hydrogen (H) contents in poly(butylene succinate-co-adipate) (PBSA) analysed by vario EL III Element Analyzer (elementar Analysensysteme GmbH, Hanau, Germany).

| Element | Content (%) |
|---|---|
| C | 56.94 |
| N | 0.000 |
| H | 7.371 |